Conductive Gold Nanoparticle Mirrors at Liquid/Liquid Interfaces

Ping-Ping Fang,[†] Shu Chen,[‡] Haiqiang Deng,[†] Micheál D. Scanlon,[†] Frédéric Gumy,[†] Hye Jin Lee,[§] Dmitry Momotenko,[†] Véronique Amstutz,[†] Fernando Cortés-Salazar,[†] Carlos M. Pereira,[⊥] Zhilin Yang,[‡] and Hubert H. Girault[†,*]

[†]Laboratoire d'Electrochimie Physique et Analytique, Ecole Polytechnique Fédérale de Lausanne, Station 6, CH-1015 Lausanne, Switzerland, [‡]Department of Physics, Xiamen University, Xiamen 361005, China, [§]Department of Chemistry and Green-Nano Materials Research Center, Kyungpook National University, 1370 Sankyuk-dong, Buk-gu, Daegu, 702-701, Republic of Korea, and [⊥]Centro de Investigação em Química—UP, L4, Departamento de Química e Bioquímica da Faculdade de Ciências, Universidade do Porto, 4169-007 Porto, Portugal

ABSTRACT Gold nanoparticle (Au NP) mirrors, which exhibit both high reflectance and electrical conductance, were self-assembled at a [heptane + 1,2-dichloroethane]/water liquid/liquid interface. The highest reflectance, as observed experimentally and confirmed by finite difference time domain calculations, occurred for Au NP films consisting of 60 nm diameter NPs and approximate monolayer surface coverage. Scanning electrochemical microscopy approach curves over the interfacial metallic NP films revealed a transition from an insulating to a conducting electrical material on reaching a surface coverage at least equivalent to the formation of a single monolayer. Reflectance and conductance transitions were interpreted as critical junctures corresponding to a surface coverage that exceeded the percolation threshold of the Au NP films at the [heptane + 1,2-dichloroethane]/water interface.

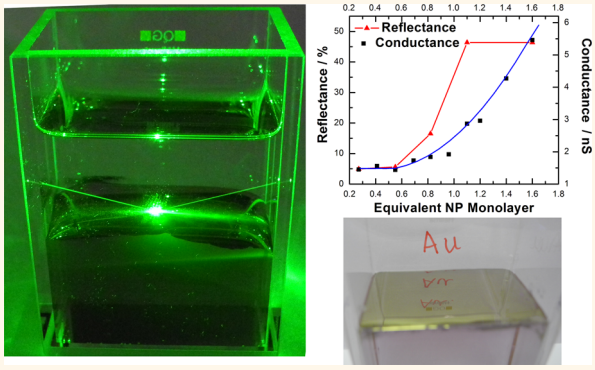

KEYWORDS: surface plasmon resonance · Au nanoparticle mirror · liquid/liquid interface · reflectance · conductance · scanning electrochemical microscopy

The development of liquid mirrors with high reflectance is a key technological challenge currently being addressed in the field of adaptive optics, with applications ranging from astronomical telescopes to smart windows.[1] One interesting, but challenging, strategy is to create a liquid nanoparticle (NP) mirror with tunable surface plasmon resonance (SPR) and electrical conductance. To this end, interfacial assemblies of NPs at liquid/liquid interfaces offer a straightforward route to form such ordered nanostructures.[2−8] Several distinct approaches to prepare interfacial self-assembled mono- and multilayers, primarily of noble metal NPs due to their interesting optical properties (*e.g.*, scattering and SPR), have been reported.[5,9] Vanmaekelbergh and co-workers reported the interfacial self-assembly of gold (Au) NPs by using charge-stabilized nanocrystal colloids at the oil/water interface.[10] Wang and co-workers investigated the self-assembly of Au NPs with different ligands.[11] Park's group developed a method to prepare close-packed NP films at the hexane/water interface in order to transfer them onto a solid substrate.[12] Several other theoretical and experimental studies have been reported to control the interfacial self-assembly of NPs.[7,11,13−23] Nevertheless, a purposely controllable assembly of NPs at a liquid/liquid interface is still difficult to accomplish,[24,25] and the reflectivity (or SPR) of NP-based mirrors at liquid/liquid interfaces has been scarcely investigated.

Scanning electrochemical microscopy (SECM) is a sensitive technique for contactless measurement of lateral charge propagation and conductivity in ultrathin films.[26] The advantages of using SECM are that the film under study does not need to be externally biased (avoiding any physical contact) and that measurements can be made at small scales (a few tens of micrometers). Therefore, SECM has been applied mainly to the characterization of NP films at solid substrates[27,28] and air/water interfaces.[29]

* Address correspondence to Hubert.Girault@epfl.ch.

Received for review July 26, 2013 and accepted September 18, 2013.

Published online September 18, 2013
10.1021/nn403879g

Longitudinal SPR experiments are usually performed for Au NP films deposited on a solid flat substrate that is optically coupled with a prism.[30,31] The SPR signal is dependent on many parameters such as the optical properties of the metals and, in the case of films prepared by assembly of NPs, on the size and shape of the NP, as well as the distance between them.[32] Thus, developing a clear understanding of the link between the interfacial microstructure and the resultant properties of the Au NP films is crucial for the development of a host of exciting technologies. For example, Turek *et al*. highlighted novel plasmonic properties of nonaggregated Au NPs adsorbed at a water/1,2-dichloroethane interface by carefully controlling the particle density and average interparticle spacing to create "plasmonic rulers".[33] Recently, Kornyshev, Urbakh, and co-workers presented rigorous theoretical analysis of both the ability to localize functionalized metal[21] or semiconductor NPs[34] at the liquid/liquid interface and the optical properties of such interfacial NP films.[19,21] This topic is termed "electrovariable nanoplasmonics" and envisioned to lead to the development of novel electro-optic devices.[34] Recently, Girault and co-workers also explored the theory of longitudinal SPR at the liquid/liquid interface and have shown that the LSPR spectra of NPs located at a liquid/liquid interface differ from those in a uniform (single-phase) environment.[35,36] Girault and co-workers have also shown that Au NP films prepared in a similar manner to those described herein are stable during potential cycling with cyclic voltammetry.[37] Thus far, such mirror-like Au NP films have been applied to enhance the photocurrent responses associated with the heterogeneous quenching of a porphyrin by ferrocene at the water/1,2-dichloroethane interface. This enhancement has been ascribed to a plasmon resonance process of the Au assembly.[37] Additionally, several recent reports have highlighted the ability of interfacial Au NP films to act as novel substrates for surface-enhanced Raman spectroscopy (SERS) applications.[38,39]

Herein, we report the preparation of reproducible interfacial liquid mirror-like structures by controlling the amount of Au NPs injected onto the oil/water interface. The surface coverage and thickness of the film may be controlled by direct tuning of the amount of NPs deposited onto the interface. In order to understand the optical properties of these Au NP films, initially the reflectance of the films as a function of angular dependence and Au NP coverage at the interface was measured and then subsequently modeled by three-dimensional finite difference time domain (FDTD) calculations. SECM studies allowed the qualitative monitoring of the transition from an insulating to an electrically conducting film as a function of Au NP surface coverage.

RESULTS AND DISCUSSION

Reflectivity of Au NP Films: Influence of Au NP Surface Coverage. The dependence of the reflectance of the interfacial Au NP films on the Au NP surface coverage was studied with 60 nm Au NPs (the optimal NP size, discussed in detail *vide infra*) using a custom-built reflectance setup; see Figure 1 and the Supporting Information SI-1 for an optical image and schematic of the reflectance setup, respectively, and see Figure 2 for the reflectance experimental data obtained. We used S-polarized light because it gave higher reflectivity (*vide infra*). The critical angle (θ_c; *i.e.*, the angle of incidence above which total internal reflection (TIR) occurs) of the employed oil/water interface was found to be 72° according to Fresnel's law.[40] Addition of pure ethanol aliquots to the liquid/liquid interface generated negligible variations on the reflectance curves (less than 1°, results not shown). However, addition of Au NPs to the interface resulted in surface coverage dependent increases of the reflectance at angles $< \theta_c$ and decreases in reflectance at angles $> \theta_c$, ascribable to an interplay between Au NP absorption effects,

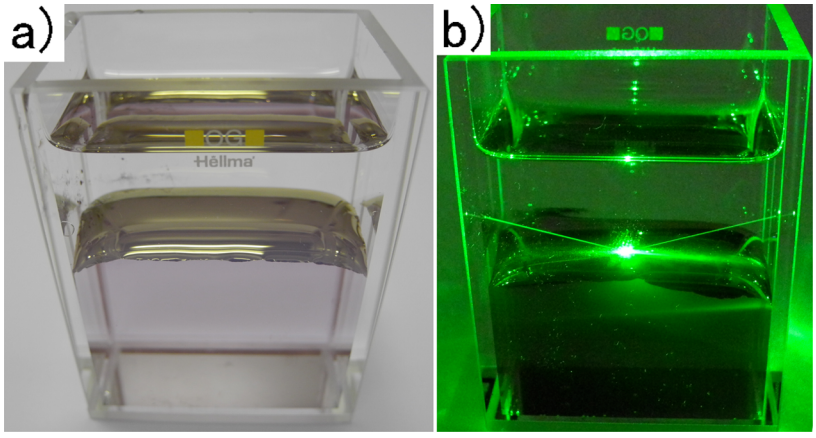

Figure 1. Optical images of Au NP films prepared at the [heptane + DCE]/water interface. These images are representative of metallic films prepared using 60 nm Au NPs with a 1.6 Au NP ML surface coverage, (a) in the absence of and (b) irradiated with laser light (λ = 532 nm). The quartz cell was silanized to render the inner surfaces hydrophobic prior to each experiment.

Au NP scattering effects, and the angle-dependent underlying reflectivity of the interface (Figure 2). Reflectance (R) can be approximately determined by eq 1:

$$R = 1 - T_{trans} - A_{ab} - S_{rest\ scattering} \quad (1)$$

where T_{trans} and A_{ab} are the transmission and absorption of light, respectively, while $S_{rest\ \ scattering}$ represents the "rest" scattering efficiency, excluding reflectance. In such a system, scattering contributes to the reflectance only when light scatters at the reflectance angle (θ_R), while both transmission and absorption clearly reduce the observed reflectance at all angles. Thus, at angles < θ_c, an increase in scattering from interfacial Au NPs at θ_R increases the observed reflectivity relative to the bare interface (where transmission dominates). However, at angles > θ_c, scattering at all angles except θ_R and absorption from interfacial Au NPs reduce the observed reflectivity relative to the bare interface (where TIR dominates).

Examining the reflectance data in more detail reveals that when 0.3 and 0.6 interfacial Au NP monolayer (ML) surface coverage was achieved, large reflectance variations were observed, particularly above θ_c (Figure 2). These variations were likely caused by the random passage of Au NP islands under the incident light beam, since there were insufficient NPs to entirely cover the interface. Moreover, when 0.8 Au NP ML surface coverage was reached, a mirror-like structure began to become apparent and observable by the naked eye. However, this film remained inhomogeneous, as indicated by the reflectance instabilities above θ_c (Figure 2). Indeed, only upon reaching 1.1 Au NP ML surface coverage did the reflectance reach a maximum value, with a clearly distinguishable Au NP mirror formed and visible without the aid of optical microscopy (Figure 1a). Such Au NP films were reflective under green laser irradiation, with some absorption and scattering occurring concurrently (Figure 1b). Injection of further Au NPs onto the interface caused no discernible changes in reflectance (*i.e.*, 1.6 Au NP ML surface coverage, Figure 2). With high NP surface coverage (*i.e.*, 1.1 and 1.6 ML) the reflectance signals above θ_c stabilized, indicating a homogeneous or compact mirror-like structure.

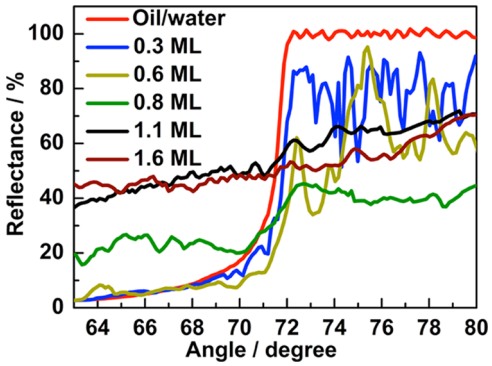

Figure 2. Experimentally observed reflectance of Au NP films, formed at the [heptane + DCE]/water interface, with varying surface coverages of 60 nm Au NPs (S-polarized light).

Influence of Light Polarization. The influence of S and P polarization on the reflectance of bare *vs* Au NP film modified liquid/liquid interfaces, using 60 nm Au NPs and an interfacial 1.1 Au NP ML surface coverage, was investigated. The experimental results clearly indicated an increased reflectance with S-polarized light in comparison to P-polarized for modified interfaces and a polarization-independent behavior for bare interfaces (Figure 3a). Such an observation may be attributed to strong SPR absorption at 532 nm with P polarization and a diminished light absorption with S polarization. Although both kinds of surface plasmons affect the far field and near field in a similar way, the excitation condition is quite different. When a compact Au NP film forms at an interface, the S-polarized light can excite only the localized surface plasmon polaritons (LSPs) mode, while the P-polarized light excites both the propagating surface plasmon polaritons (PSPs) and LSPs at the same time. Thus, more light energy will couple to the near field for P-polarized light.[41,42] In order to confirm this explanation, we carried out an FDTD simulation (Figure 3b) considering LSPs for S-polarized light and both LSPs and PSPs for P-polarized light, and indeed found an excellent match between experiment and theory. A previous work by Chen *et al.* reported similar results for S and P polarization of a

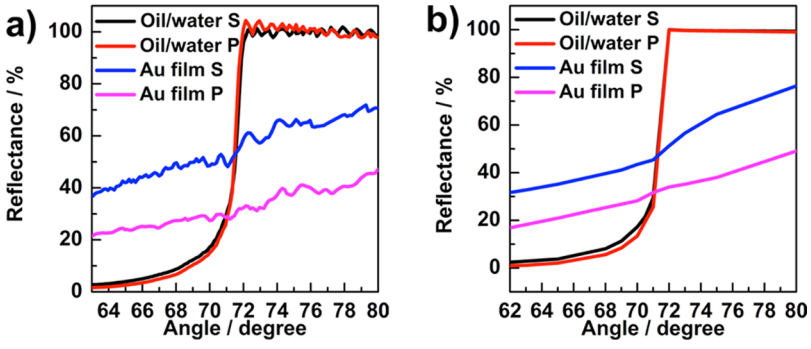

Figure 3. Experimentally observed (a) and calculated (b) reflectance of unmodified [heptane + DCE]/water interfaces and interfacial Au NP films consisting of 60 nm Au NPs with 1.6 Au NP ML surface coverages as a function of S- and P-polarized light.

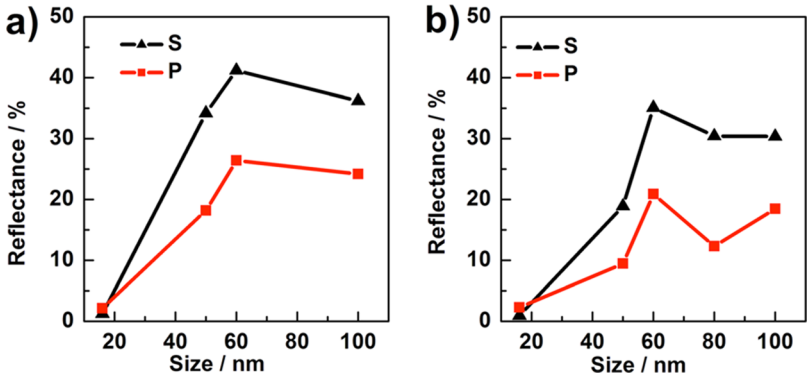

Figure 4. Experimentally observed (a) and calculated (b) reflectance of Au NP films consisting of varying NP sizes with 1.1 Au NP ML surface coverages at the [heptane + DCE]/water interface measured at 65° using 532 nm laser irradiation.

polarization-independent drop filter.[43] Therefore S-polarized light will provide a higher reflectance in comparison to P-polarized.

Influence of NP Size. A key parameter in this study warranting further investigation was the effect of Au NP size on the observed reflectance for self-assembled films. First, considering 16 nm Au NP interfacial self-assembled films, the reflectance at 65° (*i.e.*, below θ_c) was similar to that of the bare oil/water interface (Figure 4a). Subsequently, the reflectance reached a maximum with 60 nm Au NPs, while a further increase of the Au NP size to 100 nm decreased the observed reflectance. FDTD simulations confirmed that optimal reflectivity is indeed observed when utilizing 60 nm Au NPs to create the interfacial mirror-like films (Figure 4b). Furthermore, considering all NPs in this study as nanospheres, in the limit where the particles are small compared to the wavelength, their scattering (σ_{scatt}) and absorbance (σ_{abs}) cross sections have markedly different dependences on the NP radius (R), as well as other parameters such as the wavelength (λ) and the ratios of the refractive indices of the particle and the medium (m); see eqs 2 and 3:[44]

$$\sigma_{scat} = \frac{128\pi^5}{3\lambda^4} R^6 \left[\frac{m^2 - 1}{m^2 + 1}\right]^2 \quad (2)$$

$$\sigma_{abs} = -\frac{8\pi^2}{\lambda} R^3 \, \mathrm{Im}\left[\frac{m^2 - 1}{m^2 + 2}\right] \quad (3)$$

As σ_{scatt} scales with R^6, while σ_{abs} scales with R^3, the relative contribution of scattering to absorption increases quickly with NP size. Thus, in general terms, for small metal NPs light absorption predominates over scattering, whereas scattering dominates as the metal NP size increases. Thus, an optimal NP size exists for reflectivity where absorption (reducing the observed reflectivity at all angles, as discussed *vide supra*) and scattering (increasing the observed reflectivity for light scattered at θ_R, as discussed *vide supra*) counterbalance, and this is identified here as 60 nm for interfacial films of Au NPs, in good agreement with previous literature.[21]

Influence of the Wavelength of Incident Light. The dependence of the reflectance of the interfacial Au NP films on the incident light wavelength (λ_i, scanned from 300 to 800 nm) was studied as a function of interfacial Au NP surface coverage, using 60 nm Au NPs and at an angle of 0° (*i.e.*, far below θ_c). The experiments were performed using a white light source (Ocean Optics 2000 miniature fiber optic spectrometer) with a dual optical fiber capable of both shining incident light onto the Au NP film and collecting the reflected light simultaneously. The fiber was positioned vertically, directly perpendicular to the Au NP film (hence at 0°). At a low interfacial surface coverage, *i.e.*, 0.3 Au NP ML, the reflectance was independent of λ_i, Figure 5a. However, increasing the Au NP surface coverage gradually led to (a) an increased reflectance across the spectrum eventually plateauing at the highest Au NP ML coverages, analogous to earlier observations using the green laser ($\lambda = 532$ nm) below θ_c (Figure 2) and (b) a gradual narrowing of the SPR signal, due to the formation of more compact, homogeneous interfacial Au NP films. For fully compact films (*i.e.*, for surface coverages in excess of 1.1 Au NP ML using 60 nm Au NPs, as discussed earlier) the SPR peak shifted toward red wavelengths (*i.e.*, 650 nm) relative to aqueous colloidal Au NP solutions (*i.e.*, 537 nm) as a consequence of electronic coupling between individual Au NPs in the Au NP film; see Supporting Information SI-2.[31] The reflectance spectra depicted in Figure 5a can be divided into three distinct regions: (1) for 300 nm < λ_i < 500 nm, low reflectance values were recorded due to interband absorption of Au;[32] (2) for 500 nm < λ_i < 550 nm, beyond the interband absorption region, the photons cannot be absorbed, and an increase in reflectance was measured; however, this trend was interrupted in region (3), for 550 nm <λ_i < 800 nm, where a clear decrease in reflectance occurs, centered at 650 nm, due to SPR absorbance of the Au NP film.[31,32] These distinct experimental features were replicated by FDTD calculations, as shown in Figure 5b, further confirming the shift of the SPR signal for Au NPs to the red on Au NP film formation.

Electrical Conductivity of Au NP Films. To complement the reflectance studies, SECM was employed to probe

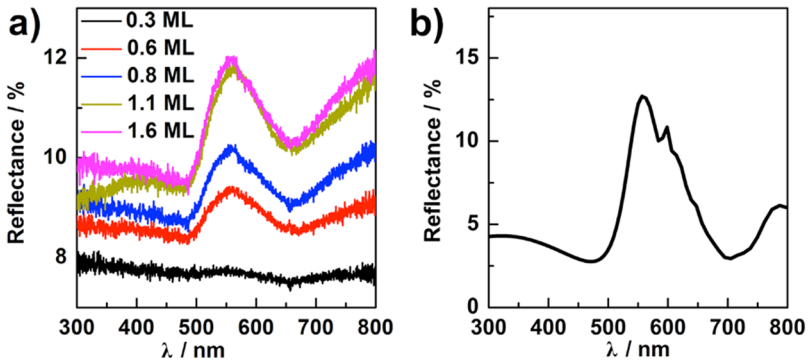

Figure 5. (a) Experimentally observed reflectance of Au NP films consisting of 60 nm Au NPs with varying surface coverages as a function of a wide range of wavelengths with an angle of 0°. (b) Calculated reflectance of a single equivalent interfacial monolayer film consisting of a 60 nm Au NP film at the [heptane + DCE]/water interface.

the electrical properties of the Au NP films. The neat aqueous phase was contacted with an organic phase consisting of a heptane/DCE solution ($V_{heptane}/V_{DCE}$ = 3:2) that contained 2 mM BATB as the supporting electrolyte and 2 mM DMFc as the redox probe molecule. Approach curve measurements were conducted by recording the steady-state diffusion-limited current (i_T) at the Pt ultramicroelectrode (UME) for the one-electron oxidation of DMFc to $DMFc^+$ as a function of distance (d) between the Pt UME and the liquid/liquid interface. While the microelectrode was moved toward the interface in a controlled motion, the potential of the tip was kept constant at +0.80 V, in order to obtain the diffusion-controlled oxidation of DMFc to $DMFc^+$. Finally, the normalized current ($i_T/i_{T,\infty}$, where $i_{T,\infty}$ is the steady-state current in the bulk solution) was plotted against the normalized distance ($L = d/a$, where d is the distance between the tip and the substrate and a is the tip radius). An inert substrate restricts the diffusion of bulk redox species toward the electroactive tip as the tip−substrate distance progressively decreases. This in turn leads to a decrease of the current profile (known as negative feedback). In contrast, conductive films allow the recycling of redox species thanks to lateral charge propagation (*i.e.*, conductivity) at the probed area of the substrate. As a consequence, when the SECM tip approaches a conductive film, an increment on the recorded current is observed.[45]

Current−distance profiles obtained by controllably approaching the Au NP film modified liquid/liquid interfaces (of varying Au NP surface coverages, as indicated) with a Pt UME are presented in Figure 6. An increase in conductivity with increasing Au NP surface coverage was indicated by a gradual transition from negative feedback to positive feedback. At surface coverages from, and in excess of, 1.1 Au NP ML a critical conductivity transition has been surpassed and may be correlated with the electrical percolation threshold under the experimental conditions tested. The conductivity continues to increase with increasing Au NP ML surface coverages from 1.1 to 1.6 ML and is associated with the formation of multilayers, *i.e.*, a 3D

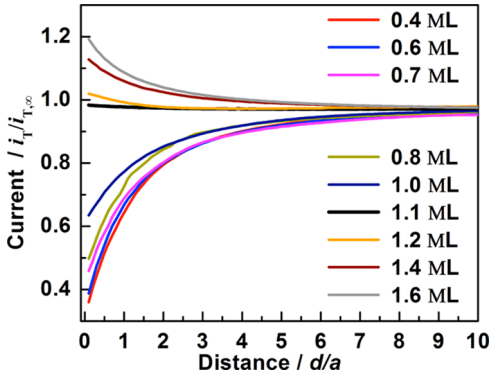

Figure 6. SECM approach curves with a Pt UME (radius, a, = 10 μm; RG = 7) to a [heptane + DCE]/water interface in the presence of different Au NP surface coverages. The oil phase contained 2 mM DMFc and 2 mM BATB. Translation rate = 1 μm s^{-1}.

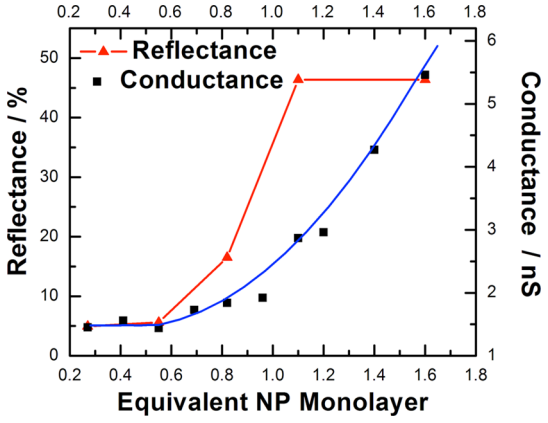

Figure 7. Comparison of the experimentally observed reflectance and calculated electrical conductance (based on the experimental data in Figure 6) of Au NP films consisting of 60 nm Au NPs with varying surface coverages at the [heptane + DCE]/water interface.

network of particles, as shown by scanning electron microscopy (SEM) (see Supporting Information SI-3).

The electrical conductivity data of interfacial 60 nm Au NP films as a function of surface coverage was calculated employing the method proposed by Unwin's group (see Supporting Information SI-4)[26] and

directly compared with the corresponding reflectance data in Figure 7. Whereas the change of reflectance occurred relatively sharply with surface coverage, the change of electric conductance was much more gradual. The initial onset of maximum reflectivity, *i.e.*, at 1.1 Au NP ML surface coverage, correlated with the transition of conductivity from negative to positive feedback. These comparative data suggest that electronic coupling leading to light reflectivity occurs at a submonolayer coverage above the percolation threshold, whereas electronic conductivity takes place once a monolayer has been reached.

CONCLUSIONS

A reflective and conductive Au NP liquid mirror has been successfully prepared at a liquid/liquid interface. The reflectivity of Au NP films, prepared with varying interfacial Au NP surface coverages and Au NP sizes, was characterized as a function of incident light angle, wavelength, and polarization both experimentally and using three-dimensional FDTD calculations. For studies carried out below the critical angle at the liquid/liquid interface, a maximum reflectivity was obtained using Au NP films prepared with 60 nm Au NPs, at a surface coverage of approximately one equivalent monolayer and using S-polarized light. The electrical conductance of the Au NP films increased progressively with the Au NP surface coverage, as indicated by scanning electrochemical microscopy studies, with a transition from insulating to conductive behavior occurring upon reaching an equivalent monolayer surface coverage. The precise mechanism of conductance is still a matter of debate, and a perspective following this study is to elucidate whether electrons are tunneling across the ligands stabilizing the NPs or if electrons conduct by NPs touching at monolayer coverage. Meanwhile, the reflectance reached a steady-state value, due to electronic coupling, at a submonolayer coverage above the percolation threshold. This study lays the fundamental groundwork toward developing conductive and reflective metallic liquid mirrors for applications in new (electro)optical devices.

EXPERIMENTAL SECTION

Chemicals. Tetrachloroauric acid ($HAuCl_4$, 99.9%) was purchased from Aldrich. Citrate trisodium dihydrate ($Na_3C_6H_5O_7 \cdot 2H_2O$), dimethyldichlorosilane, 1,2-dichloroethane (DCE), heptane, bis(triphenylphosphoranylidene)ammonium chloride (BACl), lithium tetrakis(pentafluorophenyl) borate diethyl etherate (LiTB-DEE), and decamethylferrocene (DMFc) were purchased from Fluka. All chemicals were used as received without further purification. Millipore water (18.2 MΩ·cm) was used in all experiments. The organic electrolyte bis(triphenylphosphoranylidene) ammonium tetrakis(pentafluorophenyl)borate (BATB) was synthesized as reported previously.[6]

Preparation and Characterization of Au NP Films. Au NPs with different sizes were prepared according to Frens' method by the reduction of $AuCl_4^-$ with sodium citrate.[46] The Au NPs synthesized in the present work were *ca.* 16 ± 3, 45 ± 10, 60 ± 15, and 100 ± 20 nm in diameter (henceforth denoted as 16, 45, 60, and 100 nm Au NPs, respectively), as determined by UV/visible spectroscopy (obtained on a USB 2100, Ocean Optics spectrophotometer using a quartz cuvette with a path length of 10 mm) and scanning electron microscopy (obtained using a Schottky field-emission scanning electron microscope (FEI XLF-30, Philips) operated at beam voltages between 1 and 30 kV). Beam voltages were adjusted to minimize charging effects.

The interfacial Au NP films were prepared in a rectangular quartz cell (4 cm × 2 cm × 3 cm). The surfaces of the inner walls of the quartz cell were rendered hydrophobic by silanization with dimethyldichlorosilane prior to film formation. The oil phase used was a heptane/DCE mixture ($V_{heptane}/V_{DCE}$ = 3:2), thereby forming a [heptane + DCE]/water interface. This particular oil phase was chosen as it has several attributes beneficial to our studies. First, [heptane + DCE] has a refractive index close to that of water ($n_{[heptane+DCE]}$ and n_{water} are 1.403 and 1.333, respectively, as measured by an Abbe refractometer NAR-1T SOLID model from ATAGO). Such close matching of refractive indices offers a high critical angle (θ_c; *i.e.*, the angle of incidence *above* which total internal reflection occurs) at the oil/water interface of 72° according to Fresnel's law.[40] This thereby allows us to study the effect of Au NP film formation on the reflectance of the interface over a wider range of angles (63° to 71°) below θ_c. Additionally, the [heptane + DCE] solvent is less dense than water, allowing reflective measurements from the top side, has an appropriate density to obtain a convex interface, and, finally, has a suitable dielectric constant to perform electrochemical experiments.

To form a film-like structure at the oil/liquid interface, various amounts of Au NPs suspended in ethanol were injected close to the liquid/liquid interface. A previously synthesized colloidal Au NP solution (30 mL, 0.012 wt % $HAuCl_4$) was first centrifuged, then separated from the supernatant solution, and finally redissolved in ethanol (0.8 mL). Different aliquots of this Au NP/ethanol suspension were injected at the oil/water interface to form Au NP films of different surface coverage. Au NPs were always injected from the water phase to take advantage of the lower density of ethanol in comparison to water. This facilitated the self-assembly of the Au NPs at the interface and ensured they did not remain in the bulk aqueous phase. The Au NPs spread across the interface immediately after injection. An equivalent interfacial monolayer (herein denoted ML) was estimated by quantifying the amount of Au NPs injected at the interface, the average size of the NP, and the total area of the liquid/liquid interface (see Supporting Information SI-2). According to this calculation, 1.1 ± 0.1 ML and 1.6 ± 0.1 ML equivalent monolayers of Au NPs were reached under experimental conditions where 400 and 600 μL of the Au NP/ethanol solution was injected onto the interface, respectively (see Supporting Information SI-2). An optical picture of the Au NP film prepared at a liquid/liquid interface is shown in Figure 1. The formed films were further dried and characterized by SEM (see Supporting Information SI-3).

In order to study the angular dependence of the reflectance of the Au NP films at the liquid/liquid interface, a system with two rotating arms was constructed to change precisely the angle between the arms using a linear translation stage under Labview control (see Supporting Information SI-1). The reflectance was calibrated by assuming that total reflection of the pristine oil/water interface was equal to 100%.

The conductivity of the Au NP films was probed by SECM measurements performed by a commercially available SECM instrument (CHI-900, CH Instruments, Texas, USA). A silver/silver chloride wire (Ag/AgCl in 10 mM LiCl + 1 mM BACl aqueous solution) and a Pt wire were used as the reference and counter electrode, respectively. The working electrode was a 10 μm diameter Pt UME disk with a glass insulating sheath prepared according to the literature.[47] The RG (ratio of the overall tip radius to that of the platinum disk) of the Pt UME was equal to 7,

as determined from optical micrographs. The potential applied to the working electrode was chosen according to preliminary cyclic voltammograms to achieve the mass transport controlled oxidation of the redox mediator (see Supporting Information SI-5). BATB (2 mM) was used as the supporting electrolyte and 2 mM DMFc as the redox probe molecule. We recognized as a concern the influence of salt present in the organic phase during SECM experiments, in terms of inducing aggregation of Au NPs at the interface, when carrying out these experiments. Therefore, we took the precaution of using the minimum amount of salt to allow valid SECM measurements while having no discernible influence on the Au NP absorption behavior. To this effect a salt concentration of 2 mM had no influence on the Au NP absorption behavior. SECM approach curves were obtained by approaching the prepared Au NP film at the liquid/liquid interface with a Pt UME moving at a translation rate of 1 μm/s. Analysis of the SECM approach curves performed over the different Au NP films allowed an estimation of the relationship between the film conductance and the surface coverage (see Supporting Information SI-4).

Calculations. The three-dimensional finite difference time domain method has rapidly become one of the most important computational methods in electromagnetics since Yee proposed it in 1966.[48] The basic principle of FDTD is to numerically solve Maxwell's differential equations. In the FDTD method, both space and time are divided into discrete segments. Space is segmented into box-shaped "cells" with the electric fields located on the edges of the box and the magnetic fields positioned on the faces. Every *E* component is surrounded by four *H* components, and every *H* component is surrounded by four *E* components. This orientation of the fields is known as the "Yee cell", which is the basis for any FDTD simulation. Time is quantized into small steps where each step represents the time required for the field to travel from one cell to the next. Maxwell's equations are discretized in both the time and the space domain in order to find the *E* and *H* fields at different positions and at different time steps. This method can conveniently be applied to simulating the electromagnetic scattering and radiation from a target of complex shape, as well as nonuniform dielectric objects, by simply adjusting the number, size, and material properties of the Yee cell.

3D FDTD was used to calculate the reflectivity of Au NPs located at the [heptane + DCE]/water interface (see Supporting Information SI-6). Au NPs were assumed to form a film in close proximity to each other at the interface and spread to the *xy*-plane in the FDTD simulation. Bloch boundary, periodic boundary, and perfectly matched boundary were respectively used in the *x*-, *y*-, and *z*-axes in the FDTD simulation. The amplitude of the incident electric field was chosen as 1.0 V/m. In order to maintain the accuracy and stability of the FDTD calculation, simulation times in all calculations were set to 10 ps. This was long enough to ensure calculation convergence. The Yee cell was set to $2 \times 2 \times 2$ nm^3, small enough to accurately model the Au NPs at the liquid/liquid interface. The total calculation area was 8 cm^2. The calculations were performed with commercial Lumerical FDTD solutions (version 7.5) software. From the simulation results, the reflectivity of the Au NPs on the oil/water interface as a function of the NP size, excitation wavelength, light polarization, and reflection angle was calculated.

Conflict of Interest: The authors declare no competing financial interest.

Supporting Information Available: UV/visible absorption spectra, scanning electron microscopy images, scheme of the setup for reflectance measurements, cyclic voltammetric data, details of the conductivity calculation method, and the details of the FDTD calculations are available free of charge *via* the Internet at http://pubs.acs.org.

Acknowledgment. The authors are thankful to Prof. Martin Moskovits (University of California) for valuable discussions with respect to the dependence of reflectance on the NP size. H.-Q.D. acknowledges the Chinese Scholarship Council for financial support. This work was financially supported by the SNF grant "Solar Fuels" 200 021-134 745.

REFERENCES AND NOTES

1. Borra, E. F.; Seddiki, O.; Angel, R.; Eisenstein, D.; Hickson, P.; Seddon, K. R.; Worden, S. P. Deposition of Metal Films on an Ionic Liquid as a Basis for a Lunar Telescope. *Nature* **2007**, *447*, 979–981.
2. Lin, Y.; Skaff, H.; Emrick, T.; Dinsmore, A. D.; Russell, T. P. Nanoparticle Assembly and Transport at Liquid-Liquid Interfaces. *Science* **2003**, *299*, 226–229.
3. Wang, D.; Duan, H.; Mohwald, H. The Water/Oil Interface: The Emerging Horizon for Self-Assembly of Nanoparticles. *Soft Matter* **2005**, *1*, 412–416.
4. Ranatunga, R. J. K. U.; Nguyen, C. T.; Wilson, B. A.; Shinoda, W.; Nielsen, S. O. Molecular Dynamics Study of Nanoparticles and Non-Ionic Surfactant at an Oil−Water Interface. *Soft Matter* **2011**, *7*, 6942–6952.
5. Hu, L.; Chen, M.; Fang, X.; Wu, L. Oil-Water Interfacial Self-Assembly: A Novel Strategy for Nanofilm and Nanodevice Fabrication. *Chem. Soc. Rev.* **2012**, *41*, 1350–1362.
6. Su, B.; Abid, J.-P.; Fermín, D. J.; Girault, H. H.; Hoffmannová, H.; Krtil, P.; Samec, Z. Reversible Voltage-Induced Assembly of Au Nanoparticles at Liquid|Liquid Interfaces. *J. Am. Chem. Soc.* **2003**, *126*, 915–919.
7. Hu, J.; Wu, T.; Zhang, G.; Liu, S. Efficient Synthesis of Single Gold Nanoparticle Hybrid Amphiphilic Triblock Copolymers and Their Controlled Self-Assembly. *J. Am. Chem. Soc.* **2012**, *134*, 7624–7627.
8. Wei, J.; Wang, H.; Deng, Y.; Sun, Z.; Shi, L.; Tu, B.; Luqman, M.; Zhao, D. Solvent Evaporation Induced Aggregating Assembly Approach to Three-Dimensional Ordered Mesoporous Silica with Ultralarge Accessible Mesopores. *J. Am. Chem. Soc.* **2011**, *133*, 20369–20377.
9. Qiu, P.; Jensen, C.; Charity, N.; Towner, R.; Mao, C. Oil Phase Evaporation-Induced Self-Assembly of Hydrophobic Nanoparticles into Spherical Clusters with Controlled Surface Chemistry in an Oil-in-Water Dispersion and Comparison of Behaviors of Individual and Clustered Iron Oxide Nanoparticles. *J. Am. Chem. Soc.* **2010**, *132*, 17724–17732.
10. Reincke, F.; Hickey, S. G.; Kegel, W. K.; Vanmaekelbergh, D. Spontaneous Assembly of a Monolayer of Charged Gold Nanocrystals at the Water/Oil Interface. *Angew. Chem., Int. Ed.* **2004**, *43*, 458–462.
11. Duan, H.; Wang, D.; Kurth, D. G.; Möhwald, H. Directing Self-Assembly of Nanoparticles at Water/Oil Interfaces. *Angew. Chem., Int. Ed.* **2004**, *43*, 5639–5642.
12. Park, Y.-K.; Park, S. Directing Close-Packing of Midnanosized Gold Nanoparticles at a Water/Hexane Interface. *Chem. Mater.* **2008**, *20*, 2388–2393.
13. Isa, L.; Amstad, E.; Schwenke, K.; Del Gado, E.; Ilg, P.; Kroger, M.; Reimhult, E. Adsorption of Core-Shell Nanoparticles at Liquid-Liquid Interfaces. *Soft Matter* **2011**, *7*, 7663–7675.
14. Pienpinijtham, P.; Han, X. X.; Ekgasit, S.; Ozaki, Y. An Ionic Surfactant-Mediated Langmuir-Blodgett Method to Construct Gold Nanoparticle Films for Surface-Enhanced Raman Scattering. *Phys. Chem. Chem. Phys.* **2012**, *14*, 10132–10329.
15. Grzelczak, M.; Vermant, J.; Furst, E. M.; Liz-Marzan, L. M. Directed Self-Assembly of Nanoparticles. *ACS Nano* **2010**, *4*, 3591–3605.
16. Binder, W. H. Supramolecular Assembly of Nanoparticles at Liquid−Liquid Interfaces. *Angew. Chem., Int. Ed.* **2005**, *44*, 5172–5175.
17. Kubowicz, S.; Hartmann, M. A.; Daillant, J.; Sanyal, M. K.; Agrawal, V. V.; Blot, C.; Konovalov, O.; Möhwald, H. Gold Nanoparticles at the Liquid−Liquid Interface: X-ray Study and Monte Carlo Simulation. *Langmuir* **2008**, *25*, 952–958.
18. Calzolari, D. C. E.; Pontoni, D.; Deutsch, M.; Reichert, H.; Daillant, J. Nanoscale Structure of Surfactant-Induced Nanoparticle Monolayers at the Oil−Water Interface. *Soft Matter* **2012**, *8*, 11478–11483.
19. Kornyshev, A. A.; Marinescu, M.; Paget, J.; Urbakh, M. Reflection of Light by Metal Nanoparticles at Electrodes. *Phys. Chem. Chem. Phys.* **2012**, *14*, 1850–1859.
20. Yockell-Lelievre, H.; Borra, E. F.; Ritcey, A. M.; da Silva, L. V. Optical Tests of Nanoengineered Liquid Mirrors. *Appl. Opt.* **2003**, *42*, 1882–1887.

21. Flatté, M. E.; Kornyshev, A. A.; Urbakh, M. Electrovariable Nanoplasmonics and Self-Assembling Smart Mirrors. *J. Phys. Chem. C* **2010**, *114*, 1735–1747.
22. Luo, M.; Olivier, G. K.; Frechette, J. Electrostatic Interactions to Modulate the Reflective Assembly of Nanoparticles at the Oil-Water Interface. *Soft Matter* **2012**, *8*, 11923–11932.
23. Andala, D. M.; Shin, S. H. R.; Lee, H. Y.; Bishop, K. J. M. Templated Synthesis of Amphiphilic Nanoparticles at the Liquid-Liquid Interface. *ACS Nano* **2012**, *6*, 1044–1050.
24. Yogev, D.; Efrima, S. Novel Silver Metal Liquid Like Films. *J. Phys. Chem.* **1988**, *92*, 5754–5760.
25. Gingras, J.; Déry, J.-P.; Yockell-Lelièvre, H.; Borra, E.; Ritcey, A. M. Surface Films of Silver Nanoparticles for New Liquid Films. *Colloid Surf. A: Physicochem. Eng. Asp.* **2006**, *279*, 79–86.
26. Whitworth, A. L.; Mandler, D.; Unwin, P. R. Theory of Scanning Electrochemical Microscopy (SECM) as a Probe of Surface Conductivity. *Phys. Chem. Chem. Phys.* **2005**, *7*, 356–365.
27. Ruiz, V.; Liljeroth, P.; Quinn, B. M.; Kontturi, K. Probing Conductivity of Polyelectrolyte/Nanoparticle Composite Films by Scanning Electrochemical Microscopy. *Nano Lett.* **2003**, *3*, 1459–1462.
28. Cornut, R.; Lefrou, C. New Analytical Approximation of Feedback Approach Curves with a Microdisk SECM Tip and Irreversible Kinetic Reaction at the Substrate. *J. Electroanal. Chem.* **2008**, *621*, 178–184.
29. Quinn, B. M.; Prieto, I.; Haram, S. K.; Bard, A. J. Electrochemical Observation of a Metal/Insulator Transition by Scanning Electrochemical Microscopy. *J. Phys. Chem. B* **2001**, *105*, 7474–7476.
30. Han, Y.; Corn, R. M. Characterization and Application of Surface Plasmon-Enhanced Optical Diffraction from Electrodeposited Gold Nanowire Arrays. *J. Phys. Chem. Lett.* **2011**, *2*, 1601–1606.
31. Halas, N. J.; Lal, S.; Chang, W.-S.; Link, S.; Nordlander, P. Plasmons in Strongly Coupled Nanostructures. *Chem. Rev.* **2011**, *111*, 3913–3961.
32. Earp, A. A.; Smith, G. B. Metal Nanoparticle Plasmonics inside Reflecting Metal Films. *Appl. Phys. Lett.* **2010**, *96*, 243108–3.
33. Turek, V. A; Cecchini, M. P.; Paget, J.; Kucernak, A. R.; Kornyshev, A. A.; Edel, J. B. Plasmonic Ruler at the Liquid−Liquid Interface. *ACS Nano* **2012**, *6*, 7789–7799.
34. Flatté, M. E.; Kornyshev, A. A.; Urbakh, M. Nanoparticles at Electrified Liquid−Liquid Interfaces: New Options for Electro-Optics. *Faraday Discuss.* **2009**, *143*, 109–115.
35. Yang, Z.; Chen, S.; Fang, P.; Ren, B.; Girault, H. H.; Tian, Z. LSPR Properties of Metal Nanoparticles Adsorbed at a Liquid−Liquid Interface. *Phys. Chem. Chem. Phys.* **2013**, *15*, 5374–5378.
36. Hojeij, M.; Younan, N.; Ribeaucourt, L.; Girault, H. H. Surface Plasmon Resonance of Gold Nanoparticles Assemblies at Liquid | Liquid Interfaces. *Nanoscale* **2010**, *2*, 1665–1669.
37. Schaming, D. H.; Hojeij, M.; Younan, N.; Nagatani, H.; Lee, H. J.; Girault, H. H. Photocurrents at Polarized Liquid/Liquid Interfaces Enhanced by a Gold Nanoparticle Film. *Phys. Chem. Chem. Phys.* **2011**, *13*, 17704–17711.
38. Cecchini, M. P.; Turek, V. A.; Paget, J.; Kornyshev, A. A.; Edel, J. B. Self-Assembled Nanoparticle Arrays for Multiphase Trace Analyte Detection. *Nat. Mater.* **2013**, *12*, 165–171.
39. Kim, K.; Han, H. S.; Choi, I.; Lee, C.; Hong, S.-G.; Suh, S. H.; Lee, L. P; Kang, T. Interfacial Liquid State Surface Enhanced Raman Spectroscopy. *Nat. Commun.* **2013**, *4*, 2182.
40. Doyle, W. T. Scattering Approach to Fresnel's Equations and Brewster's Law. *Am. J. Phys.* **1985**, *53*, 463–468.
41. Earp, A. A.; Smith, G. B. Evolution of Plasmonic Response in Growing Silver Thin Films with Pre-percolation Non-local Conduction and Emittance Drop. *J. Phys. D: Appl. Phys.* **2011**, *44*, 255102.
42. Schmelzer, J., Jr.; Brown, S. A.; Wurl, A.; Hyslop, M.; Blaikie, R. J. Finite-Size Effects in the Conductivity of Cluster Assembled Nanostructures. *Phys. Rev. Lett.* **2002**, *88*, 226802.
43. Chen, C.-Y.; Wang, J.-Y.; Tsai, F.-J.; Lu, Y.-C.; Kiang, Y.-W.; Yang, C. C. Fabrication of Sphere-Like Au Nanoparticles on Substrate with Laser Irradiation and their Polarized Localized Surface Plasmon Behaviors. *Opt. Express* **2009**, *17*, 14186–14198.
44. van Dijk, M. A.; Tchebotareva, A. L.; Orrit, M.; Lippitz, M.; Berciaud, S.; Lasne, D.; Cognet, L.; Lounis, B. Absorption and Scattering Microscopy of Single Metal Nanoparticles. *Phys. Chem. Chem. Phys.* **2006**, *8*, 3486–3495.
45. Oleinick, A. I.; Battistel, D.; Daniele, S.; Svir, I.; Amatore, C. Simple and Clear Evidence for Positive Feedback Limitation by Bipolar Behavior during Scanning Electrochemical Microscopy of Unbiased Conductors. *Anal. Chem.* **2011**, *83*, 4887–4893.
46. Frens, G. Controlled Nucleation for the Regulation of the Particle Size in Monodisperse Gold Suspensions. *Nat. Phys. Sci.* **1973**, *241*, 20–22.
47. Deng, H.; Peljo, P.; Cortés-Salazar, F.; Ge, P.; Kontturi, K.; Girault, H. H. Oxygen and Hydrogen Peroxide Reduction by 1,2-Diferrocenylethane at a Liquid/Liquid Interface. *J. Electroanal. Chem.* **2012**, *681*, 16–23.
48. Kane, Y. Numerical Solution of Initial Boundary Value Problems involving Maxwell's Equations in Isotropic Media. *IEEE Trans. Antennas Propag.* **1966**, *14*, 302–307.